

OPEN

DATA DESCRIPTOR

Global soil, landuse, evapotranspiration, historical and future weather databases for SWAT Applications

K. C. Abbaspour¹, S. Ashraf Vaghefi¹ , H. Yang^{1*} & R. Srinivasan²

Large-scale distributed watershed models are data-intensive, and preparing them consumes most of the research resources. We prepared high-resolution global databases of soil, landuse, actual evapotranspiration (AET), and historical and future weather databases that could serve as standard inputs in Soil and Water Assessment Tool (SWAT) models. The data include two global soil maps and their associated databases calculated with a large number of pedotransfer functions, two landuse maps and their correspondence with SWAT's database, historical and future daily temperature and precipitation data from five IPCC models with four scenarios; and finally, global monthly AET data. Weather data are 0.5° global grids text-formatted for direct use in SWAT models. The AET data is formatted for use in SWAT-CUP (SWAT Calibration Uncertainty Procedures) for calibration of SWAT models. The use of these global databases for SWAT models can speed up the model building by 75–80% and are extremely valuable in areas with limited or no physical data. Furthermore, they can facilitate the comparison of model results in different parts of the world.

Background and Summary

Soil and Water Assessment Tool (SWAT)¹ is a comprehensive hydrological model for watershed simulation. SWAT is a continuous-time, semi-distributed, and process-based model, which includes coupled upland and river processes. The land phase of SWAT includes hydrology, soil erosion, crop growth, nutrient cycling, algae transport, pesticide fate and transport, crop management, water transfer, snowfall and snowmelt, and soil temperature. The routing phase in the channels and rivers include processes such as flood routing, sediment routing, nutrient routing, pesticide routing, and routing in the reservoirs. The model is now being upgraded and restructured to SWAT+, and also coupled to glacier melt, heavy metal fate and transport, and other watershed-related processes.

SWAT is the most widely used hydrological and water quality model in the world². SWAT models are used in a variety of applications, including quantification of water resources availability^{3–10}, the impact of climate and landuse changes^{11–16}, soil erosion^{17–19}, water quality^{4,20–25}, and ecosystem services^{26–28}. SWAT also contains a modified version of the Environmental Policy Integrated Climate (EPIC) model^{29,30} for crop yield simulation^{8,12,31}. In total, more than 4,500 ISI publications can be found using SWAT on various watershed-related issues and ecosystem services around the world, which is by far the most extensive collection of such literature in the world with an average of 550 peer-reviewed publications per year in the last 4 years (data gathered from the Web of Science, October 2019).

Lack of data in many parts of the world is a severe impediment to hydrologic modeling. At the same time, much data generated on the global and local scales is also posing a modeling problem creating an additional source of uncertainty. Previous works have shown that the use of different databases for the same region leads to different model outputs and, consequently, different water resources estimates and different estimates of ecosystem variables^{4,32}. Next to model uncertainty, we have previously used the term *conditionality*^{4,33,34} to describe another constraint to a so-called calibrated model. All calibrated model parameters are uniquely conditioned on model assumptions, model structure, input data, as well as calibration data, calibration routines, and objective

¹Eawag, Swiss Federal Institute of Aquatic Science and Technology, 8600, Dübendorf, Switzerland. ²Department of Ecosystem Science and Management, Texas A & M University, College Station, TX, 77843, USA. *email: hong.yang@eawag.ch

Data Type	Resolution	Source
Soil	5 km	- FAO/UNESCO global soil map
	(1995)	http://www.fao.org/soils-portal/soil-survey/soil-maps-and-databases/faunesco-soil-map-of-the-world/en/
Soil	1 km	- Harmonized World Soil Database v 1.21
	(1995)	http://webarchive.iiasa.ac.at/Research/LUC/External-World-soil-database/HTML/index.html?sb=1
Landuse	0.3 km	- GlobCover European Space Agency
	(2004–2006)	http://due.esrin.esa.int/page_globcover.php http://www.fao.org/land-water/land/land-governance/land-resources-planning-toolbox/category/details/en/c/1036356/
Landuse	1 km	- Global Land Cover Characterization, USGS
	(1992–1993)	http://landcover.usgs.gov/glcc/ https://archive.usgs.gov/archive/sites/landcover.usgs.gov/globallandcover.html
Climate	0.5°	- Climate Research Unit (CRU)
	(1970–2005)	https://crudata.uea.ac.uk/cru/data/hrg/
Actual Evapo-transpiration	0.5°	- Remote sensing global monthly Actual Evapotranspiration dataset (NASA-MODIS)
	(1983–2006)	http://files.ntsg.umt.edu/data/ET_global_monthly_ORIG/Global_HalfDegResolution/
GCM1	0.5°	GFDL-ESM2M, daily, RCP (2.6, 4.5, 6.0, 8.5), NOAA/Geophysical Fluid Dynamics Laboratory
	(1960–2009)	https://www.isimip.org/gettingstarted/details/51/
GCM2	0.5°	HadGEM2-ES, daily, RCP (2.6, 4.5, 6.0, 8.5), Met Office Hadley Center
	(1960–2009)	https://portal.enes.org/models/earthsystem-models/metoffice-hadley-centre/hadgem2-es
GCM3	0.5°	IPSL-CM5A-LR, daily, RCP (2.6, 4.5, 6.0, 8.5), L'Institut Pierre-Simon Laplace
	(1960–2009)	https://cmc.ipsl.fr/international-projects/cmip5/
GCM4	0.5°	MIROC, daily, RCP (2.6, 4.5, 6.0, 8.5), AORI, NIES and JAMSTEC
	(1960–2009)	https://translate.google.com/translate?hl=en&sl=ja&u=http://ccsr.aori.u-tokyo.ac.jp/project.html&prev=search
GCM5	0.5°	NorESM1-M, daily, RCP (2.6, 4.5, 6.0, 8.5), Norwegian Climate Center
	(1960–2009)	https://portal.enes.org/models/earthsystem-models/ncc/noresm

Table 1. Sources and resolutions of databases available at the Pangaea and www.2w2e.com website.

function definition. A calibration program, SWAT-CUP (SWAT Calibration and Uncertainty Procedures)^{25,35}, was developed for the calibration of SWAT models. SWAT-CUP provides five different calibration routines and the option of choosing between 11 different objective functions. We have previously shown that the choice of different routines and objective functions lead to different parameters while producing equally acceptable calibration results^{36,37}. It would be desirable to always obtain unconditional model parameters independent of calibration procedures and objective functions. For this reason, in the new version of the program, we have provided an option for multi-objective calibration, which provides an option of choosing any combination of the objective functions.

Furthermore, data processing and formatting of data for different applications are highly time-consuming and prone to errors, resulting in much of the research time to be spent on data preparation instead of modeling application and analyses. For this reason, we have put together global soil, landuse, and historical and future weather databases for use in SWAT and other similar watershed models (Table 1) as described in the next section. The collection of these data provides a valuable resource for modeling, especially in regions of data scarcity.

Methods

Soil maps of the world. *FAO/UNESCO soil map of the world.* There is a general lack of reliable soil information for many parts of the world, which has significantly disadvantaged evaluation of soil erosion, land degradation, environmental impact studies, and sustainable land management programs. Two highly-used global soil maps are the FAO/UNESCO Soil Map of the World and Harmonized World Soil Database (HWSD_v121). Both maps provide a limited description of parameters, which are not directly useful for hydrologic models. We have, therefore, used pedotransfer functions developed from soils around the world to create the needed parameters such as hydraulic conductivity, available water capacity, and bulk density. Pedotransfer functions “translate data we have into data we need”³⁸. These functions estimate parameters that are difficult to measure using easily measured soil properties such as texture, color, and structure, that are routinely recorded by soil surveyors³⁹.

The FAO/UNESCO soil map of the world was prepared using the topographic map series of the American Geographical Society of New York at a nominal scale of 1:5,000,000 consisting of a 30 cm topsoil layer, and a 70 cm subsoil layer (Fig. 1). Associated files, which we produced, include “Lookup_Soil_FAO-UNESCO.txt,” which contains the correspondence between soil map and soil database, and the SWAT’s *usersoil* table in the main SWAT database “SWAT2012.mdb”.

Initially, in 2004, the first author created the soil database for the FAO/UNESCO 1995 soil map for quantification of water availability and quality in Africa^{9,10}. The soil names were created as a concatenation of the FAO mapping unit (e.g., Af14-3C) and FAO Soil-ID (e.g., 1) to give Af14-3C-1. Soil hydrologic groups were determined according to SWAT Manual⁴⁰ based on the criteria in Supplementary Table S1. The fraction of anions exclusion (ANION_EXCL) was set to 0.5 according to the SWAT Manual⁴⁰. The potential or maximum crack volume of the soil profile (SOL_CRK) expressed as a fraction of the total soil volume was set to zero as there was no information

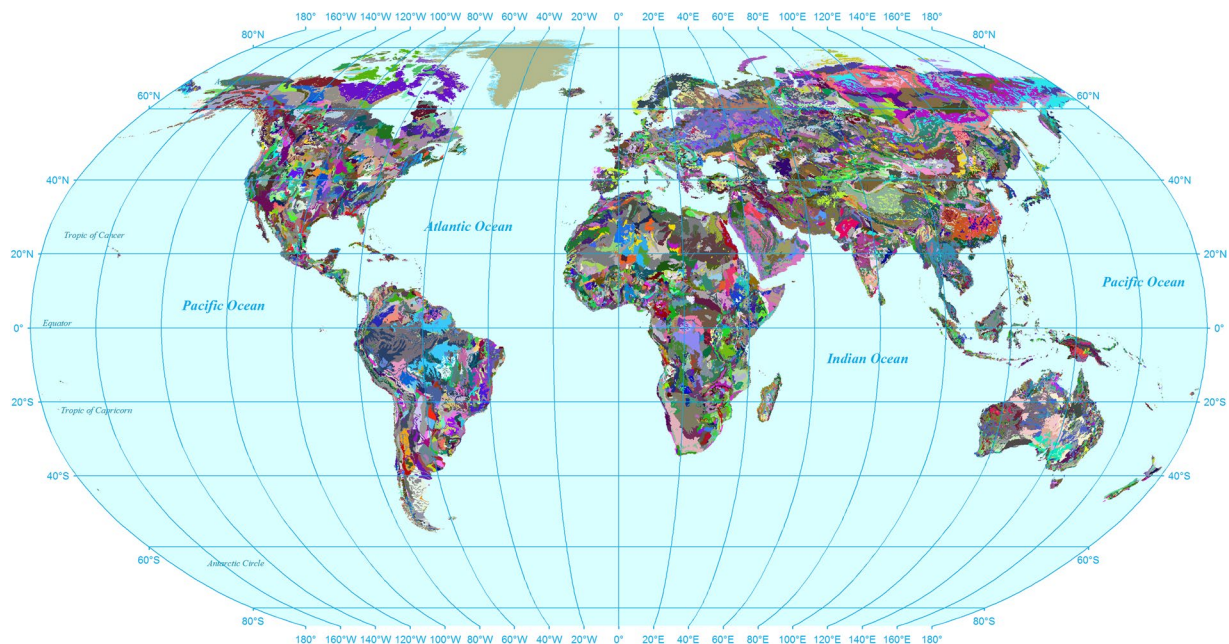


Fig. 1 Unique soil units in FAO/UNESCO Soil Map of the World.

available to evaluate this parameter. Other soil properties have initially been calculated^{9,10} using the program ROSETTA⁴¹. In the current study, we have updated this database using a large number of pedotransfer functions, as described below.

Harmonized world soil database (HWSD). The Food and Agriculture Organization of the United Nations (FAO) and the International Institute for Applied Systems Analysis (IIASA) combined the available regional and national soil information with the data already contained within the 1:5,000,000 scale FAO-UNESCO map, into a new comprehensive Harmonized World Soil Database (HWSD_v121). This map has a resolution of about 1 km (30 arc seconds) and consists of a 30-cm topsoil layer, and a 70-cm subsoil layer (Supplementary Fig. S1).

The soil variables provided in the Harmonized World Soil Database⁴² and FAO/UNESCO Soil Map of the World included soil texture (%sand, %silt, %clay), organic carbon, pH, and electrical conductivity (EC). However, from a hydrological point of view, we require parameters such as bulk density, water storage capacity, and hydraulic conductivity for different soil layers, which we used pedotransfer functions to estimate. We estimated soil bulk density (Table 2), soil available water capacity (Table 3), soil hydraulic conductivity (Table 4), soil erodibility factor for universal soil loss equation (USLE) (Table 5), and moist soil albedo (Table 6). The used pedotransfer functions are based on the soils from around the world; hence, providing parameters that are more universally applicable. The above variables were calculated for all soil records in the two soil maps.

Furthermore, to account for parameter uncertainty, the soils were sorted by their textural classes based on USDA classification⁴² that included Clay, Clay-loam, Heavy-clay, Loam, Loamy-sand, Sand, Sandy-clay, Sandy-clay-loam, Sandy-loam, Slit-loam, and Silty-clay-loam. For each textural class, we pooled the estimates of various pedotransfer functions from both FAO_UNESCO and HWSD databases and calculated their cumulative probability distributions from which we obtained parameter values at the 5%, 50%, and 95% probability levels. Values for bulk density are shown in Table 7 as an example, while other parameters are given in Supplementary Tables S2–S6. An example calculation of the 95 percent prediction uncertainty (95PPU) is shown in Supplementary Fig. S2 for the hydraulic conductivity of topsoil sandy loam. The 95PPU parameter range sets a physically meaningful limit on the parameters for different soil textural classes and is instrumental in constraining the respective parameters in model calibration. These ranges can, of course, be modified by the user as needed.

In the pre-processing of HWSD database, similar to FAO/UNESCO, we modified the data where necessary by replacing zero values of %sand, %silt, and %clay by 1, and making sure that their summation equals 100%. Also, after applying various pedotransfer functions, we replaced the negative or unreasonable values with the overall averages to avoid model-generated errors. Finally, we should point out that the soil parameters in both databases must still be calibrated for a specific location.

Landcover maps of the world. *Global land cover characterization (GLCC).* The GLCC from USGS is a landuse and land cover classification dataset based primarily on the unsupervised classification of the 1-km AVHRR (Advanced Very High-Resolution Radiometer) 10-day NDVI (Normalized Difference Vegetation Index) composites (Supplementary Fig. S3). The AVHRR source imagery dates from April 1992 through March 1993. The GLCC map contains 24 land cover types. We made the correspondence between the GLCC map units and

Bulk Density Pedotransfer Function	Reference
$\rho_b = 100/[1.72*OC/0.224 + (100 - 1.72*OC)/1.27]$	Adams ⁶⁵
$\rho_b = 1.66 - 0.308*OC^{0.5}$	Alexander ⁶⁶
$\rho_b = 1.72 - 0.294*OC^{0.5}$	Alexander ⁶⁶
$\rho_b = \exp[-2.31 - 1.079*\ln(1.72*OC/100) - 0.113*(\ln(1.72*OC/100))^2]$	Federer ⁶⁷
$\rho_b = \exp[-2.39 - 1.316*\ln(1.72*OC/100) - 0.167*(\ln(1.72*OC/100))^2]$	Huntington <i>et al.</i> ⁶⁸
$\rho_b = \exp[0.263 - 0.147*\ln(OC) - 0.103*(\ln(OC))^2]$	Huntington <i>et al.</i> ⁶⁸
$\rho_b = 1.51 - 0.113*OC$	Manrique and Jones ⁶⁹
$\rho_b = 1.66 - 0.318*OC^{0.5}$	Manrique and Jones ⁶⁹
$\rho_b = 0.111*1.450/[1.450*(1.72*OC/100) + 0.111*(1 - 1.72*OC/100)]$	Federer <i>et al.</i> ⁷⁰
$\rho_b = 1.524 - 0.0046*C - 0.051*OC - 0.0045*pH + 0.001*S$	Bernoux <i>et al.</i> ⁷¹
$\rho_b = 1.398 - 0.042*OC - 0.0047*C$	Bernoux <i>et al.</i> ⁷¹
$\rho_b = 1.578 - 0.054*OC - 0.006*T - 0.004*C$	Tomasella and Hodnett ⁷²
$\rho_b = 1.70398 - 0.00313*S + 0.00261*C - 0.11245*OC$	Leonavičiute ⁷³
$\rho_b = 1.07256 + 0.032732*\ln(S) + 0.038753*\ln(C) + 0.078886*\ln(S) - 0.054309*\ln(OC)$	Leonavičiute ⁷³
$\rho_b = 0.244*1.640/[1.640*1.72*OC/100 + 0.244*(1 - 1.72*OC/100)]$	Post and Kwon ⁷⁴
$\rho_b = \exp(0.313 - 0.191*OC + 0.02102*C - 0.000476*C^2 - 0.00432*T)$	Kaur <i>et al.</i> ⁷⁵
$\rho_b = 0.120*1.400/[1.4*1.72*OC/100 + 0.120*(1 - 1.72*OC/100)]$	Tremblay <i>et al.</i> ⁷⁶
$\rho_b = \exp(-1.81 - 0.892*\ln(1.72*OC/100) - 0.092*(\ln(1.72*OC/100))^2)$	Prevost ⁷⁷
$\rho_b = 0.159*1.561/[1.561*(1.72*OC/100) + 0.159*(1 - (1.72*OC/100))]$	Prevost ⁷⁷
$\rho_b = 1.5688 - 0.0005*C - 0.0090*OC$	Benites <i>et al.</i> ⁷⁸
$\rho_b = -1.977 + 4.105*(1.72*OC/100) - 1.229*\ln(1.72*OC/100) - 0.103*(\ln(1.72*OC/100))^2$	Perie and Ouimet ⁷⁹
$\rho_b = 0.111*1.767/[1.767*1.72*OC/100 + 0.111*(1 - 1.72*OC/100)]$	Perie and Ouimet ⁷⁹
$\rho_b = \exp(0.5379 - 0.0653*(10*1.72*OC)^{0.5})$	Han <i>et al.</i> ⁸⁰
$\rho_b = 1.02 - 0.156*\ln(1.72*OC)$	Hong <i>et al.</i> ⁸¹
$\rho_b = 0.071 + 1.322*\exp(-0.0715*OC)$	Hossain <i>et al.</i> ⁸²

Table 2. Soil Bulk Density (ρ_b) pedotransfer function (g cm^{-3}). OC = %organic carbon, C = %clay, T = %silt, S = %sand.

SWAT's (*crop*) database in Supplementary Table S7 based on the description of the land covers provided by the maps and the SWAT landuse definitions.

Global landuse GlobCover. The GlobCover is a European Space Agency initiative to develop global composites and land cover maps using observations from the 300-m MERIS sensor onboard the ENVISAT satellite mission (Supplementary Fig. S4). The GlobCover map covers the period of December 2004 to June 2006 and is derived by automatic and regionally-tuned classification of a MERIS full resolution surface reflectance time series. The GlobCover map contains 23 land cover types. We made correspondence between the GlobCover units and SWAT's (*crop*) database in Supplementary Table S8 based on the description of the land covers provided by the maps and the SWAT landuse definitions.

The databases for the above two global landuse maps are supported by the table (*crop*) in the SWAT2012.mdb database and the lookup tables "Lookup_Landuse_GlobCover.txt" and Lookup_Landuse_USGS.txt. However, similar to the soil parameters, landuse parameters must be calibrated for a given location.

Historical weather data. The historical (1970–2005) reanalysis temperature and precipitation data from the Research Unit East Anglia (CRU TS 3.1)⁴³ were reformatted from NetCDF into SWAT-readable text files. The database is daily and has a resolution of 0.5° and covers the entire globe in 67,420 files.

Future weather data. We provide five global climate models (GCM), each with four carbon evolution scenarios supported by ISI-MIP5 (Inter-Sectoral Impact Model Intercomparison Project)⁴⁴. These daily data cover the period of 1950–2099 and have a resolution of 0.5°. Similar to CRU, they have been reformatted from NetCDF into SWAT-formatted text files.

The five GCM models include HadGEM2-ES, IPSL-CM5A-LR, MIROC-ESM-CHEM, GFDL-ESM2M, and NorESM1-M (Table 1) with Representative Concentration Pathway (RCP) scenarios (RCP2.6, RCP4.5, RCP6.0, and RCP8.5)⁴⁵. The 0.5° grid WATCH Forcing Data⁴⁶ for the period of January 1, 1960, to December 31, 1999 (the reference period) was used as observation data to downscale the five GCMs⁴⁴. WATCH is a combination of the ERA-40 daily data, the 40-year reanalysis of the European Centre for Medium-Range Weather Forecasts, and the Climate Research Unit TS2.1 dataset (CRU)⁴³. The WATCH Forcing Data data combines the daily statistics of ERA-40 with the monthly mean characteristics of CRU and Global Precipitation Climatology Centre (GPCC) datasets and represents a complete gridded observational dataset for bias correction of global climate data⁴⁴.

The historical and future data can be downloaded for any given geographic location from www.2w2e.com using the template illustrated in Supplementary Fig. S5. The Climate Change Toolkit (CCT) program⁴⁷ is linked to the above databases and can be used for bias correction if local data is available. CCT uses additive correction

Available Water Capacity Pedotransfer Function	Source
$\theta_{33} = 0.1183 + 0.0096 * C - 0.00008 * C^2$	Petersen <i>et al.</i> ⁸³
$\theta_{1500} = 0.0174 + 0.0076 * C - 0.00005 * C^2$	
$\theta_{33} = 0.2081 + 0.0045 * C + 0.0013 * T - 0.0595 * \rho_b$	Hall <i>et al.</i> ⁸⁴
$\theta_{1500} = 0.0148 + 0.0084 * C - 0.000055 * C^2$	
$\theta_{33} = 0.003075 * S + 0.005886 * T + 0.008039 * C + 0.001284 * OC - 0.1434 * \rho_b$	Gupta & Larson ⁸⁵
$\theta_{1500} = 0.000059 * S + 0.001142 * T + 0.005766 * C + 0.001326 * OC + 0.02671 * \rho_b$	
$\theta_{33} = 0.2576 - 0.002 * S + 0.0036 * C + 0.0299 * OC$	Rawls <i>et al.</i> ⁸⁶
$\theta_{1500} = 0.0260 + 0.005 * C + 0.0158 * OC$	
$\theta_{33} = 0.3486 - 0.0018 * S + 0.0039 * C + 0.0228 * OC - 0.0738 * \rho_b$	Rawls <i>et al.</i> ⁸⁷
$\theta_{1500} = 0.0854 - 0.0004 * S + 0.0044 * C + 0.0122 * OC - 0.0182 * \rho_b$	
$\theta_{33} = 0.3862 - 0.0000479 * S - 0.000019 * (S/T)^2$	Rajkai & Varallyay ⁸⁸
$\theta_{1500} = 0.0139 + 0.0036 * C + 0.006508 * OC^2$	
$\theta_{33} = 0.01 * \rho_b * (2.65 + 1.105 * C - 0.01896 * C^2 + 0.0001678 * C^3 + 15.12 * \rho_b - 6.745 * \rho_b^2 - 0.1975 * C * \rho_b)$	Canarache ⁸⁹
$\theta_{1500} = 0.01 * \rho_b * (0.2805 * C + 0.0009615 * C^2)$	
$AWC = 0.000976 * C + 0.001875 * T + 0.004694 * OC$	Batjes ⁹⁰
$AWC = 0.001082 * C + 0.001898 * T + 0.007705 * OC$	Batjes ⁹⁰
$\theta_{33} = 0.04046 + 0.00426 * T + 0.00404 * C$	Tomasella & Hodnett ⁷²
$\theta_{1500} = 0.0091 + 0.00150 * T + 0.00396 * C$	
$x = -0.837531 + 0.430183 * OC$	Rawls <i>et al.</i> ⁹¹
$y = -1.40744 + 0.0661969 * C$	
$z = -1.51866 + 0.0393284 * S$	
$\theta_{33} = 0.297528 + 0.103544 * (0.0461615 + 0.290955 * x - 0.0496845 * x^2 + 0.00704802 * x^3 + 0.269101 * y - 0.176528 * x * y + 0.0543138 * x^2 * y + 0.1982 * y^2 - 0.060699 * y^3 - 0.320249 * z - 0.0111693 * x^2 * z + 0.14104 * y * z + 0.0657345 * x * y * z - 0.102026 * y^2 * z - 0.04012 * z^2 + 0.160838 * x * z^2 - 0.121392 * y * z^2 - 0.0616676 * z^3)$	
$\theta_{1500} = 0.142568 + 0.0736318 * (0.06865 + 0.108713 * x - 0.0157225 * x^2 - 0.017059 * y^2 + 0.00102805 * x^3 + 0.886569 * y - 0.223581 * x * y + 0.0126379 * x^2 * y + 0.013526 * x * y^2 - 0.0334434 * y^3 - 0.0535182 * z - 0.0354271 * x * z - 0.00261313 * x^2 * z - 0.154563 * y * z - 0.0160219 * x * y * z - 0.0400606 * y^2 * z - 0.104875 * z^2 + 0.0159857 * x * z^2 - 0.0671656 * y * z^2 - 0.0260699 * z^3)$	
$\beta = -0.00251 * S + 0.00195 * C + 0.0064 * OC + 0.000035 * S * OC - 0.00016 * C * OC + 0.0000452 * S * C + 0.299$	Saxton and Rawls ⁹²
$\gamma = -0.00024 * S + 0.00487 * C + 0.0035 * OC + 0.00029 * S * OC - 0.0000756 * C * OC + 0.0000068 * S * OC + 0.031$	
$\theta_{33} = \beta + (1.283 * \beta^2 - 0.374 * \beta - 0.015)$	
$\theta_{1500} = \gamma + (0.14 * \gamma - 0.02)$	Aina & Periaswamy ⁹³
$\theta_{33} = 0.0055 * (C + T) - 0.0013 * S * \rho_b + 0.1288$	
$\theta_{1500} = 0.0031 * C + 0.0213$	Dijerman ⁹⁴
$\theta_{33} = 0.3697 - 0.0035 * S$	
$\theta_{1500} = 0.0074 + 0.0039 * C$	Arruda <i>et al.</i> ⁹⁵
$\theta_{33} = [0.0029 * (C + T) + 0.0993] * \rho_b$	
$\theta_{1500} = [0.0027 * (C + T) + 0.0107] * \rho_b$	

Table 3. Available Water Capacity, $AWC(= \theta_{33} - \theta_{1500})$ (cm cm^{-1}) pedotransfer functions. θ_{33} = soil water content at field capacity, θ_{1500} = soil water content at wilting point, C = %clay, ρ_b = bulk density (g cm^{-3}), T = %silt, OC = %organic carbon, S = %sand.

for temperature and a multiplicative correction factor for precipitation. The program can also be used for extreme climate analysis⁴⁸.

Global actual evapotranspiration data. Actual evapotranspiration (AET) from the earth's land surface is collected by NASA using satellite data from 1982 to 2003^{49,50} (Supplementary Fig. S6). The algorithm calculates canopy transpiration and soil evaporation using a modified Penman-Monteith approach with biome-specific canopy conductance determined from the normalized difference vegetation index (NDVI). Priestley-Taylor approach was used to quantify open water evaporation. The observations from 34 flux network (FEUXNET) tower sites⁵¹ were used to parameterize an NDVI-based canopy conductance model to validate the global ET algorithm using measurements from 48 additional, independent flux towers^{49,50}.

AET has been used before to calibrate SWAT when other observed data is not available⁵². It is crucial to have a measure of AET when calibrating a SWAT model with river discharge data. Using river discharge alone, we can confidently estimate runoff and infiltration. However, components of the infiltrated water cannot be estimated with any degree of confidence. These components include soil moisture (S), aquifer recharge (AR), and actual evapotranspiration (AET) (Fig. 2). Using an estimate of AET in calibration can significantly increase our confidence in the other components of infiltrating water.

To use the provided MODIS-NASA data for calibration in SWAT-CUP, users, should overlay the MODIS-AET grids with the subbasin map of their ArcSWAT/QSWAT project and average the AET grid points inside each subbasin to one single value to represent the subbasin's AET.

Hydraulic Conductivity Pedotransfer Function	Source
$K_s = 60.96 \cdot 10^{(-0.884 + 0.0153 \cdot S)}$	Cosby <i>et al.</i> ⁹⁶
$K_s = 60.96 \cdot 10^{(-0.6 + 0.0126 \cdot S - 0.0064 \cdot C)}$	Cosby <i>et al.</i> ⁹⁶
$K_s = 24.0 \cdot \exp(12.012 - 0.0755 \cdot S + \alpha)$	Saxton <i>et al.</i> ⁹⁷
$\alpha = (-3.895 + 0.03671 \cdot S - 0.1103 \cdot C + 0.00087546 \cdot C^2) / \theta_s$	
$\theta_s = 0.332 - 0.0007251 \cdot S + 0.1276 \cdot \log(C)$	
$K_s = 339.0 \cdot (1.3 / \rho_b)^{(1.3 \cdot \beta)} \cdot \exp(-0.0688 \cdot C - 0.0363 \cdot T - 0.025)$	Campbell and Shiozawa ⁹⁸
$\gamma = \exp\{0.01 \cdot [\ln(1.025) \cdot S + \ln(0.026) \cdot T + \ln(0.001) \cdot C]\}$	
$\mu = \exp\{0.01 \cdot [\ln(1.025)]^2 \cdot S + [\ln(0.026)]^2 \cdot T + [\ln(0.001)]^2 \cdot C - [\ln(\gamma)]^2\}^{0.5}$	
$\beta = [\gamma^{\lambda} - 0.5 + 0.2 \cdot \mu]^{\lambda - 1}$	Saxton and Rawls ⁹²
$K_s = 4632(\theta_s - \theta_{33})^{3 - \lambda}$	
$\theta_s = \theta_{33} - 0.064 - 0.00097 \cdot S + 1.636(0.00278 \cdot S + 0.00034 \cdot C + 0.0128 \cdot OC - 0.000104 \cdot S \cdot OC - 0.000157 \cdot C \cdot OC - 0.0000584 \cdot S \cdot C + 0.078)$	
$\lambda = [\ln(\theta_{33}) - \ln(\theta_{1500})] / [\ln(1500) - \ln(33)]$	
$\theta_{33} = \beta + (1.283 \cdot \beta^{\lambda} - 0.374 \cdot \beta - 0.015)$	
$\beta = -0.00251 \cdot S + 0.00195 \cdot C + 0.0064 \cdot OC + 0.000035 \cdot S \cdot OC - 0.00016 \cdot C \cdot OC + 0.0000452 \cdot S \cdot C + 0.299$	
$\theta_{1500} = \gamma + (0.14 \cdot \gamma - 0.02)$	
$\gamma = 0.00024 \cdot S + 0.00487 \cdot C + 0.0035 \cdot OC + 0.00029 \cdot S \cdot OC - 0.0000756 \cdot C \cdot OC + 0.0000068 \cdot S \cdot C + 0.031$	Rawls and Brakensiek ⁹⁹
$\theta_s = 1 - \rho_b / 2.65$	
$K_s = 24 \cdot \exp(\alpha)$	
$\alpha = 19.52348 \cdot \theta_s - 8.96847 - 0.028212 \cdot C + 0.00018107 \cdot (S^{\wedge}2) - 0.0094125 \cdot (C^{\wedge}2) - 8.395215 \cdot (\theta_s^{\wedge}2) + 0.077718 \cdot S \cdot \theta_s - 0.00298 \cdot (S^{\wedge}2) \cdot (\theta_s^{\wedge}2) - 0.01949 - 2 \cdot (C^{\wedge}2) \cdot (\theta_s^{\wedge}2) + 0.0000173 \cdot (S^{\wedge}2) \cdot C + 0.02733 \cdot (C^{\wedge}2) \cdot \theta_s + 0.001434 \cdot (S^{\wedge}2) \cdot \theta_s - 0.0000035 \cdot S \cdot (C^{\wedge}2)$	Woesten <i>et al.</i> ¹⁰⁰
$K_s = \exp(\alpha)$	
$\alpha = 7.755 + 0.0352 \cdot T + 0.93(\text{topsoil}) - 0.967 \cdot (\rho_b^{\wedge}2) - 0.000484 \cdot C^{\wedge}2 - 0.000322 \cdot (T^{\wedge}2) + 0.001 \cdot T - 0.129 / OC - 0.643 \cdot \ln(T) - 0.01398 \cdot \rho_b \cdot C - 0.0973 \cdot \rho_b \cdot OC + 0.02986(\text{topsoil}) \cdot C - 0.03305 \cdot (\text{topsoil}) \cdot T$	Weynants <i>et al.</i> ¹⁰¹
$K_s = \exp(\alpha)$	
$\alpha = 1.9582 + 0.0308 \cdot S - 0.6142 \cdot \rho_b - 0.01566 \cdot OC$	

Table 4. Soil Hydraulic Conductivity (cm day⁻¹) pedotransfer functions. θ_{33} = soil water content at field capacity, θ_{1500} = soil water content at wilting point, C = %clay, ρ_b = bulk density (g cm⁻³), T = %silt, OC = %organic carbon, S = %sand, topsoil = an ordinal variable having the value of 1 for (depth 0–30 cm) or 0 (depth > 30 cm).

Soil Erodibility Pedotransfer Function	Source
$K_{USLE} = E_s \cdot E_{C-T} \cdot E_{OC} \cdot E_{HS}$	Williams ³⁰
Where:	
$E_s = 0.2 + 0.3 \cdot \exp[-0.256 \cdot S \cdot (1 - T/100)]$	
$E_{C-T} = [T / (C + T)]^{0.3}$	
$E_{OC} = 1 - (0.25 \cdot OC / (OC + \exp(0.72 - 2.95 \cdot OC)))$	
$E_{HS} = 1 - \{0.7 \cdot (1 - S/100) / [(1 - S/100) + \exp(-5.51 + 22.9 \cdot (1 - S/100))]\}$	

Table 5. Soil erodibility factor (cm day⁻¹) pedotransfer function. S = %sand, T = %silt, C = %clay, OC = %organic carbon.

Albedo Pedotransfer Function	Source
$\text{Albedo} = 0.1807 + 0.1019 \cdot \exp(-3.53 \cdot \theta_{33})$	Wang <i>et al.</i> ¹⁰²
$\text{Albedo} = 0.15 + 0.31 \cdot \exp(-12.7 \cdot \theta_{33})$	Gascoïn <i>et al.</i> ¹⁰³
$\text{Albedo} = 0.26 + 0.1068 \cdot \exp(-4.9 \cdot \theta_{33})$	Sugathan <i>et al.</i> ¹⁰⁴

Table 6. Moist Soil Albedo based on the water content at field capacity (θ_{33}).

Data Records

The Global FAO/UNESCO Soil Map of the World and associated SWAT data files (Lookup Table and SWAT2012.mdb)⁵³ are deposited at *Pangaea* and www.2w2e.com sites. There are 4,931 soil records in this data set.

The Harmonized World Soil map and associated SWAT data files (Lookup Table and SWAT2012.mdb)⁵⁴ are deposited at *Pangaea* and www.2w2e.com sites. There are 16,328 soil records in this data set.

The Global Land Cover Characterization (GLCC) map from USGS and SWAT data file (Lookup Table and SWAT2012.mdb)⁵⁵ are deposited at *Pangaea* and www.2w2e.com sites. There are 24 landcover types in this database.

Topsoil Bulk density (g cm ⁻³)	5% prob. Level	50% prob. Level	95% prob. Level	Subsoil Bulk density (g cm ⁻³)	5% prob. Level	50% prob. Level	95% prob. Level
Clay (2324)	0.80	1.19	1.58	Clay (2221)	1.19	1.34	1.49
Clay-loam (3034)	1.03	1.30	1.57	Clay-loam (4936)	1.19	1.37	1.55
Heavy-clay (284)	1.04	1.21	1.38	Heavy-clay (548)	1.21	1.32	1.42
Loam (6612)	0.98	1.26	1.54	Loam (5150)	1.08	1.34	1.61
Loamy-sand (1171)	1.11	1.30	1.49	Loamy-sand (1072)	1.31	1.40	1.50
Sand (918)	1.33	1.41	1.49	Sand (793)	1.38	1.41	1.44
Sandy-clay (136)	1.10	1.27	1.44	Sandy-clay (461)	1.15	1.39	1.62
Sandy-clay-loam (2463)	1.19	1.34	1.49	Sandy-clay-loam (2518)	0.97	1.36	1.74
Sandy-loam (3040)	1.08	1.32	1.57	Sandy-loam (2533)	1.14	1.37	1.60
Silt-loam (864)	0.79	1.19	1.60	Silt-loam (608)	0.74	1.26	1.77
Silty-clay (120)	0.88	1.17	1.47	Silty-clay (142)	1.04	1.32	1.59
Silty-cla-loam (95)	0.95	1.21	1.47	Silty-cla-loam (89)	1.19	1.36	1.53

Table 7. Average and uncertainty estimates of bulk density for top and subsoil based on the textural classes. The numbers in the brackets are the number of samples.

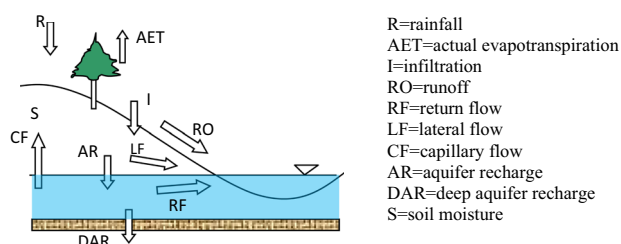


Fig. 2 Schematic illustration of the conceptual water balance model in SWAT.

The GlobCover from the European Space Agency and associated data files (Lookup Table and SWAT2012.mdb)⁵⁶ are deposited at *Pangaea* and www.2w2e.com sites. There are 23 landcover types in this database.

The historical CRU and future GCM weather data⁵⁷ are deposited at *Pangaea* and www.2w2e.com.

Finally, the Global Actual Evapotranspiration Data⁵⁸ in text format is deposited at *Pangaea* and www.2w2e.com.

Technical Validation

The global soil and landuse databases have been successfully used in many SWAT applications around the world^{4,6,9,10,16,59–62}. Validation of these maps, which are based on satellite observations, are offered by ground-truth observations conducted by the map developers and also in various literature^{63,64}.

There is a significant variation in the reported values of soil parameters in the literature and by various agencies. In this research, we used a large number of pedotransfer functions and soil samples from around the world to estimate the textural-based soil parameters. In Table 8 we compared our estimated values of bulk density and hydraulic conductivity with values reported by the U.S. Department of Agriculture (USDA), STRUCTx (STRUCTURAL ENGINEERING RESOURCES website, see Table 8), and other reported values. The rest of the parameters could not be found based on textural classes. As evident, there are significant variations in all estimates, especially for saturated hydraulic conductivities. For this reason, it is essential to have a range of estimates, so one can limit the values to a likely range during model calibration.

Usage Notes

There are 4,931 soil records in the FAO/UNESCO database, and 16,328 records in the HWSD soil map. Both (*usersoil*) tables are in the SWAT2012.mdb database. The field (*Name*) is concatenated by using the fields SU-SYM74, SU-SYM90, MU_GLOBAL, and ISSOL as given in the original HWSD database. SU-SYM74 is the soil unit symbol according to the FAO-74 soil classification, SU-SYM90 is the soil unit symbol according to the FAO-90 soil classification, MU_GLOBAL is the Global Mapping Unit identifier, which provides the link between the GIS soil units and the attribute database, and ISSOL is a field indicating if the soil mapping unit is a soil (1) or a non-soil (0). All maps provided have the World WGS-84 Spatial Reference without any projection. The users will have to project these maps as needed before using it in the ArcSWAT or QSWAT models.

Different soil and landuse maps are provided to emphasize the fact that often more than one database is available for building and calibrating a model, and also to encourage the users to use different databases to realize the *conditionality* of their calibrated models. Calibrated model parameters are always conditioned on the input data, meaning one could obtain a different set of parameters if one had used a different set of available data. This is probably the most disappointing aspect of calibration.

Topsoil Bulk density (g cm ⁻³)	5% prob. Level	50% prob. Level	95% prob. Level	USDA*	STRUCTx**	From Articles***
Clay (2324)	0.80	1.21	1.58	1.4	1.33	—
Clay-loam (3034)	1.03	1.26	1.57	1.45	1.39	1.44–1.59
Heavy-clay (284)	1.04	1.30	1.38	1.3	—	—
Loam (6612)	0.98	1.41	1.54	1.5	1.43	1.28–1.60
Loamy-sand (1171)	1.11	1.27	1.49	1.6	1.43	1.33–1.82
Sand (918)	1.33	1.34	1.49	1.65	1.43	1.27–1.75
Sandy-clay (136)	1.10	1.32	1.44	1.4	1.47	1.55–1.65
Sandy-clay-loam (2463)	1.19	1.19	1.49	1.5	1.5	1.49–1.75
Sandy-loam (3040)	1.08	1.17	1.57	1.55	1.46	1.4–1.76
Silt-loam (864)	0.79	1.21	1.60	1.5	1.38	1.12–1.61
Silty-clay (120)	0.88	1.16	1.47	1.45	1.26	0.95–1.33
Silty-clay-loam (95)	0.95	1.23	1.47	1.5	1.3	0.86–1.60
* https://www.nrcs.usda.gov/wps/portal/nrcs/detail/soils/survey/office/ssr10/tr/?cid=nrcs144p2_074844						
** https://structx.com/Soil_Properties_002.html						
***Ranges from ¹⁰⁵ & https://hort.ifas.ufl.edu/woody/critical-value.shtml &						
Topsoil Saturated Hydraulic Conductivity (mm hr ⁻¹)	5% prob. Level	50% prob. Level	95% prob. Level	USDA*	STRUCTx**	From articles (SD)***
Clay	3	5	13	2–5	5	40 (255)
Clay-loam	6	9	13	5–15	9	13 (46)
Heavy-clay	3	3	6	2–5	—	—
Loam	8	12	22	15–51	25	58 (113)
Loamy-sand	70	101	130	151–508	562	98 (133)
Sand	111	117	176	151–508	634	330 (328)
Sandy-clay	10	15	26	2–5	8	27 (83)
Sandy-clay-loam	12	19	44	5–15	23	32 (170)
Sandy-loam	20	47	78	51–152	124	49 (183)
Silt-loam	7	10	54	15–51	26	52 (96)
Silty-clay	3	4	4	2–5	4	—
Silty-clay-loam	3	4	7	2–5	6	180 (434)
* https://www.nrcs.usda.gov/wps/portal/nrcs/detail/soils/survey/office/ssr10/tr/?cid=nrcs144p2_074846						
** https://structx.com/Soil_Properties_007.html						
***Based on García-Gutiérrez <i>et al.</i> ¹⁰⁶						

Table 8. Comparison of the values of bulk density and saturated hydraulic conductivity estimated in this research with values reported by different sources.

A calibrated model is, therefore, always: non-unique, subjective, conditional, and subsequently limited on the scope of its use. To achieve *unconditionality*, the calibrated parameters must be integrated over all conditioning factors. Hence, we recommend using different physical inputs and multi-objective calibration procedures.

Received: 22 May 2019; Accepted: 21 October 2019;

Published online: 06 November 2019

References

1. Arnold, J. G. *et al.* SWAT: model use, calibration, and validation. *T. ASABE* **55**, 1491–1508 (2012).
2. Gassman, P. W., Sadeghi, A. M. & Srinivasan, R. Applications of the SWAT Model Special Section: Overview and Insights. *J. Environ. Qual* **43**, 1–8 (2014).
3. Cuceloglu, G., Abbaspour, K. C. & Ozturk, I. Assessing the Water-Resources Potential of Istanbul by Using a Soil and Water Assessment Tool (SWAT) Hydrological Model. *Water* **9**, 814 (2017).
4. Abbaspour, K. C., Rouholahnejad, E., Vaghefi, S., Srinivasan, R. & Klöve, B. Modelling hydrology and water quality of the European Continent at a subbasin scale: calibration of a high-resolution large-scale SWAT model. *J. Hydrol.* **524**, 733–752 (2015).
5. Zuo, D. *et al.* Simulating spatiotemporal variability of blue and green water resources availability with uncertainty analysis. *Hydrol. Process.* **29**, 1942–1955 (2015).
6. Rouholahnejad, E., Abbaspour, K. C., Srinivasan, R., Bacu, V. & Lehmann, A. A high resolution spatiotemporal distribution of water resources quantity and quality in the Black Sea Basin. *Water Resour. Res.* **50**, 5866–5885 (2014).
7. Narsimlu, B., Gosain, A. K. & Chahar, B. R. Assessment of Future Climate Change Impacts on Water Resources of Upper Sind River Basin, India Using SWAT Model. *Water Resour. Manag* **27**, 3647–3662 (2013).
8. Sun, C. & Ren, L. Assessing crop yield and crop water productivity and optimizing irrigation scheduling of winter wheat and summer maize in the Haihe plain using SWAT model. *Hydrol. Process.* **28**, 2478–2498 (2014).
9. Schuol, J., Abbaspour, K. C., Srinivasan, R. & Yang, H. Estimation of freshwater availability in the West African Sub-continent using the SWAT hydrologic model. *J. Hydrol.* **352**, 30–49 (2008).
10. Schuol, J., Abbaspour, K. C., Srinivasan, R. & Yang, H. Modelling Blue and Green Water Availability in Africa at monthly intervals and subbasin level. *Water Resour. Res.* **44**, W07406 (2008).

11. Rouholahnejad, E. F., Abbaspour, K. C. & Lehmann, A. Water Resources of the Black Sea Catchment under Future Climate and Landuse Change Projections. *Water* **9**, 598 (2017).
12. Vaghefi, S. A., Abbaspour, K. C., Faramarzi, M., Srinivasan, R. & Arnold, J. G. Modeling Crop Water Productivity Using a Coupled SWAT-MODSIM Model. *Water* **9**, 157 (2017).
13. Vaghefi, S., Mousavi, S. J., Abbaspour, K. C., Srinivasan, R. & Yang, H. Analyses of the impact of climate change on water resources components, drought and wheat yield in semiarid regions: Karkheh River Basin in Iran. *Hydrol. Process.* **28**, 2018–2032 (2014).
14. Zuo, D., Xu, Z., Zhao, J., Abbaspour, K. C. & Yang, H. Response of runoff to climate change in the Wei River basin, China. *Hydrol. Sci. J* **60**, 508–522 (2015).
15. Zhang, X., Xu, Y. P. & Fu, G. Uncertainties in SWAT extreme flow simulation under climate change. *J. Hydrol.* **515**, 205–222 (2014).
16. Abbaspour, K. C., Faramarzi, M., Ghasemi, S. & Yang, H. Assessing the impact of climate change on water resources in Iran. *Water Resour. Res.* **45**, W10434 (2009).
17. Abdelwahab, O. M., Ricci, G. F., De Girolamo, A. M. & Gentile, F. Modelling soil erosion in a Mediterranean watershed: Comparison between SWAT and AnnAGNPS models. *Env. Res* **166**, 363–376 (2018).
18. Melaku, N. D. *et al.* Prediction of soil and water conservation structure impacts on runoff and erosion processes using SWAT model in the northern Ethiopian highlands. *J. Soils Sediments* **18**, 1743–1755 (2018).
19. Rostamian, R. *et al.* Application of SWAT Model for Estimating Runoff and Sediment in a Mountainous Watershed in Central Iran. *Hydrol. Sci* **53**, 977–988 (2008).
20. Seo, M., Jaber, F., Srinivasan, R. & Jeong, J. Evaluating the Impact of Low Impact Development (LID) Practices on Water Quantity and Quality under Different Development Designs Using SWAT. *Water* **9**, 193 (2017).
21. Merwade, V., Baffaut, C., Bieger, K., Boithias, L. & Rathjens, H. Featured Series Introduction: SWAT Applications for Emerging Hydrologic and Water Quality Challenges. *J. Am. Water Resour. As* **53**, 67–68 (2017).
22. Singh, G. & Saraswat, D. Development and evaluation of targeted marginal land mapping approach in SWAT model for simulating water quality impacts of selected second generation biofeedstock. *Environ. Modell. & Softw* **81**, 26–39 (2016).
23. Rocha, J., Roebeling, P. & Rial-Rivas, M. E. Assessing the impacts of sustainable agricultural practices for water quality improvements in the Vouga catchment (Portugal) using the SWAT model. *Sci. Total Environ* **536**, 48–58 (2015).
24. Baffaut, C., Sadler, E. J., Ghidry, F. & Anderson, S. Long-Term agroecosystem research in the Central Mississippi River Basin: SWAT simulation of flow and water quality in the Goodwater Creek Experimental Watershed. *J. Environ. Qual* **44**, 84–96 (2015).
25. Abbaspour, K. C. *et al.* Modelling hydrology and water quality in the pre-alpine/alpine thur watershed using swat. *J. Hydrol.* **333**, 413–430 (2007).
26. Zarrineh, N., Abbaspour, K. C., van Griensven, A., Jeangros, B. & Holzkamper, A. Model-Based Evaluation of Land Management Strategies with Regard to Multiple Ecosystem Services. *Sustainability* **10**, 3844 (2018).
27. Karabulut, A. *et al.* Mapping water provisioning services to support the ecosystem-water-food-energy nexus in the Danube river basin. *Ecosys. Serv* **17**, 278–292 (2016).
28. Notter, B., Hurni, H., Wiesmann, U. & Abbaspour, K. C. Modelling water provision as an ecosystem service in a large East African river basin. *Hydrol. Earth Syst. Sc* **16**, 69–86 (2012).
29. Kamali, B., Abbaspour, K. C., Lehmann, A., Wehrli, B. & Yang, H. Uncertainty-based auto-calibration for crop yield – the EPIC+ procedure for a case study in Sub-Saharan Africa. *Eur. J. Agron.* **93**, 57–72 (2018).
30. Williams, J. R. The EPIC Model in *Computer Models of Watershed Hydrology* Chapter 25 (Water Resources Publications, Highlands Ranch, CO, 1995).
31. Fereidoon, M. & Koch, M. SWAT-MODSIM-PSO optimization of multi-crop planning in the Karkheh River Basin, Iran, under the impacts of climate change. *Sci. Total Environ.* **630**, 502–516 (2018).
32. Kamali, B., Abbaspour, K. C. & Yang, H. Assessing the Uncertainty of Multiple Input Datasets in the Prediction of Water Resource Components. *Water* **9**, 709 (2017).
33. Abbaspour, K. C., Sonnleitner, M. & Schulin, R. Uncertainty in Estimation of Soil Hydraulic Parameters by Inverse Modeling: Example Lysimeter Experiments. *Soil Sci. Soc. of Am. J* **63**, 501–509 (1999).
34. Abbaspour, K. C., Vaghefi, S. A. & Srinivasan, R. A guideline for successful calibration and uncertainty analysis for soil and water assessment: A review of papers from the 2016 International SWAT Conference. *Water* **10**, 6 (2018).
35. Abbaspour, K. C., Johnson, A. & van Genuchten, M. Th. Estimating uncertain flow and transport parameters using a sequential uncertainty fitting procedure. *Vadose Zone J.* **3**, 1340–1352 (2004).
36. Yang, J., Reichert, P., Abbaspour, K. C. & Yang, H. Comparing uncertainty analysis techniques for a SWAT application to Chaohe Basin in China. *J. Hydrol.* **358**, 1–23 (2008).
37. Houshmand, D., Esmaili, K., Faridhosseini, A., Sanaei Nejad, H., Khalili, D. & Abbaspour, K. C. Sensitivity of calibrated parameters and water resource estimates on different objective functions and optimization algorithms. *Water* **9**, 384 (2017).
38. Bouma, J. Using soil survey data for quantitative land evaluation. *Adv. Soil Sci* **9**, 177–213 (1989).
39. Abbaspour, K. C. & Moon, D. E. Relationship between conventional field information and some soil properties measured in the laboratory. *Geoderma* **55**, 119–140 (1992).
40. Neitsch, S. L., Arnold, J. G., Kiniry, J. R. & Williams, J. R. Soil and Water Assessment Tool User's Manual, version 2000. (Grassland, Soil and Water Research Laboratory, Agricultural Research Service, Blackland Research Center, Texas Agricultural Experiment Station 2001).
41. Schaap, M. G., Leij, F. J. & van Genuchten, M. T. ROSETTA: a computer program for estimating soil hydraulic parameters with hierarchical pedotransfer functions. *J. Hydrol.* **251**, 163–176 (2001).
42. Harmonized World Soil Database. Coordinated by: Nachtergaele, F. *et al.* (FAO, IIASA, ISRIC, ISSCAS, JRC 2009).
43. Harris, I., Jones, P. D., Osborn, T. J. & Lister, D. H. Updated high-resolution grids of monthly climatic observations - the CRU TS3.10 Dataset. *Int. J. Climatol.* **34**, 623–642 (2014).
44. Hempel, S., Frieler, K., Warszawski, L., Schewe, J. & Piontek, F. A trend-preserving bias correction - the ISI-MIP approach. *Earth Syst. Dyn* **4**, 219e236 (2013).
45. Moss, R. H. *et al.* The next generation of scenarios for climate change research and assessment. *Nature* **463**, 747–756 (2010).
46. Weedon, G. P. *et al.* Creation of the watch forcing data and its use to assess global and regional reference crop evaporation over land during the twentieth century. *J. Hydrometeorol.* **12**, 823–848 (2011).
47. Vaghefi, S. A., Abbaspour, N., Kamali, B. & Abbaspour, K. C. A toolkit for climate change analysis and pattern recognition for extreme weather conditions - Case study: California-Baja California Peninsula. *Environ. Modell. & Softw.* **96**, 181–198 (2017).
48. Vaghefi, S. A. *et al.* The future of extreme climate in Iran. *Sci. Rep* **9**, 1464 (2019).
49. Zhang, K. *et al.* Satellite based analysis of northern ET trends and associated changes in the regional water balance from 1983 to 2005. *J. Hydrol.* **379**, 92–110 (2009).
50. Zhang, K., Kimball, J. S., Nemani, R. R. & Running, S. W. A continuous satellite-derived global record of land surface evapotranspiration from 1983 to 2006. *Water Resour. Res.* **46**, W09522 (2010).
51. Baldocchi, D. Breathing of the terrestrial biosphere: Lessons learned from a global network of carbon dioxide flux measurement systems. *Aust. J. Bot.* **56**, 1–26 (2008).
52. Odusanya, A. E. *et al.* Multi-site calibration and validation of SWAT with satellite-based evapotranspiration in a data-sparse catchment in southwestern Nigeria. *Hydrol. Earth Syst. Sci.* **23**, 1113–1144 (2019).

53. Abbaspour, K. & Saeid, A. V. Global FAO/UNESCO Soil Map of the World reformatted with SWAT format. *PANGAEA*, <https://doi.org/10.1594/PANGAEA.901313> (2019).
54. Abbaspour, K. & Saeid, A. V. Harmonized World Soil Database in SWAT Format. *PANGAEA*, <https://doi.org/10.1594/PANGAEA.901309> (2019).
55. Abbaspour, K. & Saeid, A. V. Global Land Cover for SWAT “Global Landuse USGS”. *PANGAEA*, <https://doi.org/10.1594/PANGAEA.901311> (2019).
56. Abbaspour, K. & Saeid, A. V. Global Land Cover for SWAT “Global Landuse GlobCover”. *PANGAEA*, <https://doi.org/10.1594/PANGAEA.901310> (2019).
57. Abbaspour, K. & Saeid, A. V. CRU and GCM data for SWAT model. *PANGAEA*, <https://doi.org/10.1594/PANGAEA.901312> (2019).
58. Abbaspour, K., Saeid, A. V., Lehmann, A. & Raghavan, S. Monthly actual evapotranspiration satellite data with SWAT and SWAT-CUP format. *PANGAEA*, <https://doi.org/10.1594/PANGAEA.897170> (2019).
59. Ginanjar, M. R. & Putra, S. S. Sediment trapping analysis of flood control reservoirs in Upstream Ciliwung River using SWAT Model. 2nd transdisciplinary research on environmental problems in southeast Asia. *Earth Env. Sci* **71**, 012014 (2017).
60. Asl-Rousta, B. & Mousavi, S. J. A TOPSIS-based multicriteria approach to the calibration of a basin-scale SWAT hydrological model. *Water Resour. Manag.* **33**, 439–452 (2019).
61. Kangsabanik, S. & Murmu, S. Rainfall-runoff modelling of Ajay river catchment using SWAT model. 7th International Conference on Environment and Industrial Innovation. *Earth Env. Sci.* **67**, 012033 (2017).
62. El-Sadek, A. & İrvem, A. Evaluating the impact of land use uncertainty on the simulated streamflow and sediment yield of the Seyhan River basin using the SWAT model. *Turk. J. Agric. For.* **38**, 515–530 (2014).
63. Nakaegawa, T. Comparison of Water-Related Land Cover Types in Six 1-km Global Land Cover Datasets. *Hydrol. Earth Syst. Sci.* **13**, 649–664 (2012).
64. Frey, K. E. & Smith, L. C. How well do we know northern land cover? Comparison of four global vegetation and wetland products with a new ground-truth database for West Siberia. *Global Biogeochem. CY* **21**, GB1016 (2007).
65. Adams, W. A. The effect of organic matter on the bulk and true densities of some uncultivated podzolic soils. *Soil Sci* **24**, 10Y17 (1973).
66. Alexander, E. B. Bulk densities of California soils in relation to other soil properties. *Soil Sci. Soc. Am. J* **44**, 689Y692 (1980).
67. Federer, C. A. Nitrogen mineralization and nitrification: Depth variation in four New England forest soils. *Soil Sci. Soc. Am. J* **47**, 1008Y1014 (1983).
68. Huntington, T. G., Johnson, C. E., Johnson, A. H., Siccama, T. G. & Ryan, D. F. Carbon, organic matter and bulk density relationships in a forested Spodosol. *Soil Sci.* **148**, 380Y386 (1989).
69. Manrique, L. A. & Jones, C. A. Bulk density of soils in relation to soil physical and chemical properties. *Soil Sci. Soc. Am. J* **55**, 476–481 (1991).
70. Federer, C. A., Turcotte, D. E. & Smith, C. T. The organic fraction/bulk density relationship and the expression of nutrient content in forest soils. *Can. J. For. Res.* **23**, 1026Y1032 (1993).
71. Bernoux, M., Arrouays, D., Cerri, C., Volkoff, B. & Jolivet, C. Bulk densities of Brazilian Amazon soils related to other soil properties. *Soil Sci. Soc. Am. J* **62**, 743–749 (1998).
72. Tomasella, J. & Hodnett, M. G. Estimating soil water retention characteristics from limited data in Brazilian Amazonia. *Soil Sci.* **163**, 190–202 (1998).
73. Leonavičiute, N. Predicting soil bulk and particle densities by pedotransfer functions from existing soil data in Lithuania. *Geografijos metraštis* **33**, 7–330 (2000).
74. Post, W. M. & Kwon, K. C. Soil carbon sequestration and land-use change: Processes and potential. *Glob Change Biol* **6**, 317Y327 (2000).
75. Kaur, R., Kumar, S. & Gurung, H. P. A pedo-transfer function (PTF) for estimating soil bulk density from basic soil data and its comparison with existing PTFs. *Aust. J. Soil Res.* **40**, 847Y857 (2002).
76. Tremblay, S., Ouimet, R. & Houle, D. Prediction of organic carbon content in upland forest soils of Quebec, Canada. *Can. J. For. Res.* **32**, 1Y12 (2002).
77. Prevost, M. Predicting soil properties from organic matter content following mechanical site preparation of forest soils. *Soil Sci. Soc. Am. J* **68**, 943Y949 (2004).
78. Benites, V. M., Machado, P. L. O. A., Fidalgo, E. C. C., Coelho, M. R. & Madari, B. E. Pedotransfer functions for estimating soil bulk density from existing soil survey reports in Brazil. *Geoderma* **139**, 90Y97 (2007).
79. Perie, C. & Ouimet, R. Organic carbon, organic matter and bulk density relationships in boreal forest soils. *Can. J. Soil Sci.* **88**, 315Y325 (2008).
80. Han, G. Z., Zhang, G. L., Gong, Z. T. & Wang, G. F. Pedotransfer Functions for Estimating Soil Bulk Density in China. *Soil Sci.* **177**, 158–164 (2012).
81. Hong, S. Y., Minasny, B., Han, K. H., Kim, Y. & Lee, K. Predicting and mapping soil available water capacity in Korea. *Peer J.* **1**, e71 (2013).
82. Hossain, M. F., Chen, W. & Zhang, Y. Bulk density of mineral and organic soils in the Canada’s arctic and sub-arctic. *Inf. Proc. Agric.* **2**, 183–190 (2015).
83. Petersen, G. W., Cunningham, R. L. & Matelski, R. P. Moisture characteristics of Pennsylvania soils: I. Moisture retention as related to texture. *Soil Sci. Soc. Am. J* **32**, 271–275 (1968).
84. Hall, D. G. M., Reeve, M. J., Thomasson, A. J. & Wright, V. F. Water retention, porosity and density of field soils. Tech. Monogr. 9, Soil Survey of England and Wales, Harpenden, United Kingdom (1977).
85. Gupta, S. C. & Larson, W. E. Estimating soil water retention characteristics from particle size distribution, organic matter content, and bulk density. *Water Resour. Res.* **15**, 1633–1635 (1979).
86. Rawls, W. J., Brakensiek, D. L. & Saxton, K. E. Estimation of soil water properties. *T. ASAE* **25**, 1316–1320 (1982).
87. Rawls, W. J., Brakensiek, D. L. & Soni, B. Agricultural management effects on soil water processes. I: Soil water retention and Green-Ampt parameters. *T. ASAE* **26**, 1747–1752 (1983).
88. Rajkai, K. & Varallyay, G. Estimating soil water retention from simpler properties by regression techniques. Proceedings of the International Workshop on Indirect Methods for Estimating the Hydraulic Properties of Unsaturated Soils (eds van Genuchten, M. Th., Leij, F. J. & Lund, L.), University of California, Riverside, 417–426 (1992).
89. Canarache, A. Physical-technological maps - A possible product of soil survey for direct use in agriculture. *Soil Technol.* **6**, 3–16 (1993).
90. Batjes, N. H. Development of a world data set of soil water retention properties using pedotransfer rules. *Geoderma* **71**, 31–52 (1996).
91. Rawls, W. J., Pachepsky, Y. A., Ritchie, J. C., Sobecki, T. M. & Bloodworth, H. Effect of soil organic carbon on Soilwater retention. *Geoderma* **116**, 61–76 (2003).
92. Saxton, K. E. & Rawls, W. J. Soil water characteristic estimates by texture and organic matter for hydrologic solutions. *Soil Sci. Soc. Amer. J* **70**, 1569–1578 (2006).
93. Aina, P. O. & Periaswamy, S. P. Estimating available water-holding capacity of Western Nigerian soils from soil texture and bulk density using core and sieved samples. *Soil Sci.* **140**, 55–58 (1985).

94. Dijkerman, J. An Ustult-Aquult-Tropept catena in Sierra Leone, W. Africa, II. Land qualities and land evaluation. *Geoderma* **42**, 29–49 (1988).
95. Arruda, F. B., Julio, J. Jr. & Oliveira, J. B. Parametros de solo para calculo de agua disponivel com base na textura do solo. *Rev. Bras. Cienc. Solo* **11**, 11–15 (1987).
96. Cosby, B. J., Hornberger, G. M., Clapp, R. B. & Ginn, T. R. A statistical exploration of the relationships of soil moisture characteristics to the physical properties of soils. *Water Resour. Res.* **20**, 682–690 (1984).
97. Saxton, K. E., Rawls, W. J., Romberger, J. S. & Papendick, R. I. Estimating generalized soil water characteristics from texture. *Soil Sci. Soc. Am. J* **50**, 1031–1036 (1986).
98. Campbell, G. S. & Shiozawa, S. Prediction of hydraulic properties of soils using particle size distribution and bulk density data. Indirect Methods for Estimating the Hydraulic Properties of Unsaturated Soils, (eds van Genuchten, M. Th., Leij, F. J. & Lund, L. J.), U.S. Salinity Laboratory, Riverside, CA, 317–328 (1992).
99. Rawls, W. J. & Brakensiek, D. L. Prediction of soil water properties for hydrologic modeling. Proceedings of Watershed Management in the Eighties. Denver, CO, ASCE, 293–299 (1985).
100. Woesten, J. H. M., Lilly, A., Nemes, A. & Le Bas, C. Development and use of a database of hydraulic properties of European soils. *Geoderma* **90**, 169–185 (1999).
101. Weynants, M., Vereecken, H. & Javaux, M. Revisiting Vereecken pedotransfer functions: Introducing a closed-form hydraulic model. *Vadose Zone J.* **8**, 86–95 (2009).
102. Wang, K. C. *et al.* Variation of surface albedo and soil thermal parameters with soil moisture content at a semi-desert site on the western Tibetan plateau. *Boundary Layer Meteorol* **116**, 117–129 (2005).
103. Gascoïn, S., Ducharne, A., Ribstein, P., Perroy, E. & Wagnon, P. Sensitivity of bare soil albedo to surface soil moisture on the moraine of the Zongo glacier (Bolivia). *Geophys. Res. Lett.* **36**, L02405 (2009).
104. Sugathan, N., Biju, V. & Renuka, G. Influence of soil moisture content on surface albedo and soil thermal parameters at a tropical station. *J. Earth Syst. Sci.* **123**, 1115–1128 (2014).
105. Arkhangelskaya, T. & Lukyashchenko, K. Estimating soil thermal diffusivity at different water contents from easily available data on soil texture, bulk density, and organic carbon content. *Biosystem Engineering* **168**, 83–95 (2018).
106. García-Gutiérrez, C., Pachepsky, Y. & Martín, M. A. Technical note: Saturated hydraulic conductivity and textural heterogeneity of soils. *Hydrol. Earth Syst. Sci.* **22**, 3923–3932 (2018).

Acknowledgements

The authors wish to acknowledge the support of Swiss Federal Institute of Aquatic Science and Technology (Eawag) in publishing this paper.

Author contributions

K.C.A., H.Y. and R.S. developed the concept, K.C.A. created soil parameters using pedotransfer functions, S.A.V. prepared figures and reformatted climate data in text form, K.C.A. and R.S. interpreted soil and landuse data. All authors edited and participated in manuscript preparation.

Competing interests

The authors declare no competing interests.

Additional information

Supplementary information is available for this paper at <https://doi.org/10.1038/s41597-019-0282-4>.

Correspondence and requests for materials should be addressed to H.Y.

Reprints and permissions information is available at www.nature.com/reprints.

Publisher's note Springer Nature remains neutral with regard to jurisdictional claims in published maps and institutional affiliations.



Open Access This article is licensed under a Creative Commons Attribution 4.0 International License, which permits use, sharing, adaptation, distribution and reproduction in any medium or format, as long as you give appropriate credit to the original author(s) and the source, provide a link to the Creative Commons license, and indicate if changes were made. The images or other third party material in this article are included in the article's Creative Commons license, unless indicated otherwise in a credit line to the material. If material is not included in the article's Creative Commons license and your intended use is not permitted by statutory regulation or exceeds the permitted use, you will need to obtain permission directly from the copyright holder. To view a copy of this license, visit <http://creativecommons.org/licenses/by/4.0/>.

The Creative Commons Public Domain Dedication waiver <http://creativecommons.org/publicdomain/zero/1.0/> applies to the metadata files associated with this article.

© The Author(s) 2019